Changes in extreme events over Asia for present and future climate conditions based on a modelling analysis of atmospheric circulation anomalies

Article

Accepted Version

Changes in extreme events over Asia for present and future climate conditions based on a modelling analysis of atmospheric circulation anomalies

Ranjeet S. Sokhi[1], P. R. Tiwari[1*], Joanna S.N. de Medeiros[1], Gerd A. Folberth[2] and William J. Collins[3]

[1]Centre for Atmospheric and Climate Physics Research, University of Hertfordshire, Hatfield, UK

[2]UK Met Office Hadley Centre, Exeter, UK

[3]Department of Meteorology, University of Reading, Reading, UK

*Correspondence
Dr. P. R. Tiwari
Centre for Atmospheric and Climate Physics Research,
University of Hertfordshire, United Kingdom
Email: p.r.tiwari@herts.ac.uk

Abstract

Synoptic weather and larger scale circulation patterns are closely coupled and have a major influence on regional weather and extreme events. This study examines the role of regional circulations on meteorology and extreme events for the present and future years over Asia with the WRF model driven by HadGEM2 global model boundary conditions that includes RCP4.5 scenarios based bicentennial transient simulation. The regional scale analysis was based on boundary conditions derived from 40 years of global model outputs spanning periods of 1995-2005, 2015-2025, 2025-2035 and 2045-2055. For brevity these periods are labelled as 2000, 2020, 2030, 2050 and 'represent' decadal periods centered around the named years. Model results were compared and validated (using a number of skill metrics) against observations for the present period showing that the model is able to delineate the observed features within 95% confidence level compared to the annual mean. To characterise and quantify the changes in the circulation patterns, an Empirical Orthogonal Function (EOF) based analysis was conducted. Results indicate that wintertime minimum temperatures are projected to increase by *3 - 4 ^0C* over Asia by 2050 compared to reference period of 2000. Furthermore, anti-cyclonic activity associated with low PV anomalies and high positive temperature anomalies may be a key driver that influence the increase in frequency and duration of heat waves and droughts over SA, SEA, EA and NA regions of Asia. Overall, the modelling results suggest that regional meteorology and circulation patterns may significantly influence extremes over Asia in the future. Such impacts will have major implications for weather patterns as well as for air pollution over the region both of which will require policy responses to adjust to a changing regional climate.

Key words: Asia, Regional climate, Extremes, Prediction.

1. Introduction

Studies are showing that extreme events, such as floods, heat waves, cold surges and winter storms can have profound impacts on both the natural environment and human society (Trenberth et al. 2003; Ulbrich et al. 2003; Trigo 2006; Barriopedro et al. 2011; Dole et al. 2011; Flato et al. 2013; Kumar et al. 2015). Consequently, understanding the impact of synoptic weather and large-scale circulation on regional weather and extreme events is crucial for improving prediction of regional meteorology and potential hazards (Panda et al. 2016; Rohini et al. 2016, Dileepkumar et al. 2018; Maharana et al. 2020). Development of effective mitigation strategies and policies depend on such information for tackling impact of air pollution and climate change which is becoming increasingly important for regions with rising population and industrialisation.

Numerous studies have investigated the potential relationship between circulation and weather extremes. In particular, a number of studies have focussed on quantifying temperature extremes over Europe (Yiou and Nogaj 2004; Cassou et al. 2005; Santos and Corte-Real 2006; Della-Marta et al. 2007; Andrade et al. 2012). Some studies have examined the relationship between temperature and precipitation extremes, and the large-scale circulation variability (Sillmann et al. 2011; Buehler et al. 2011; Pattnayak et al. 2016) highlighting the important role of the North Atlantic Oscillation (NAO), atmospheric blocking, extra tropical cyclones and their influence on colder and wetter winters and hotter and dryer summers. These findings are not only pertinent to the European region but also to most of the Northern Hemisphere, including the Asian continent. However, there are relatively few published articles focussing on the understanding of large-scale circulation patterns and extreme weather events over the Asian region (Li et al. 2019; Tiwari et al. 2017; Kar et al. 2014).

Blocking type circulations have been found to be responsible for persistent summertime precipitation extremes over central and eastern China from 1951 to 2010 (Chen and Zhai 2013). In

January 2008 for example, southern and central China were struck by icy winter conditions due to a persistent blocking due to the Siberian High which advected cold dry air into the regions. Patterns of large-scale atmospheric circulations that dominate the either the prolonged or extreme drought in North China have been documented in recent studies such as Zhang et al. (2018, 2017). Similar studies on the large-scale atmospheric circulation that dominate the drought in southeastern periphery of the Tibetan Plateau and the extreme heat event in central and eastern China have been documented by Ma et al. (2017a,b). You et al. (2011) have examined the changes of the large-scale atmospheric circulation and proposed that a strengthening of anti-cyclonic circulation, an increasing geopotential height and a rapid warming over the Eurasian continent contributed to the changes in climate extremes in China from 1961 to 2003. The above studies indicated that there is strong coupling between regional weather, regional atmospheric circulations and extreme events. In addition, with the unique topography and geographical extension, the meteorology over the Asian region is particularly complicated.

The need of a comprehensive study over the Asian region, not only for temperature extremes, but also for wind and precipitation extremes, is of crucial scientific importance to improve our understanding of the multiple scale interactions. These types of studies are also particularly important to policy makers because of implications for mitigation against effects of air pollution, extreme weather and climate change. Furthermore, the results of this work will be useful for both weather and air quality forecasting.

The present work examines the role of regional circulation on meteorology and extreme events in a changing climate over Asia. It focuses on the following three key science questions:

(i) Which atmospheric circulation anomalies are associated with extreme weather events over Asia?

(ii) How does the spatial distribution of these anomalies influence the frequency and intensity of local weather extremes?

(iii) What changes do we expect in the future, focussing on extreme events?

A brief description of the model, data used and the methodology is provided in section 2. Results and discussions are provided in section 3 and the key findings and conclusions from this study are given in section 4.

2. Methodology

2.1 Modelling approach and data used: For the purposes of the present analysis, dynamical modelling framework is employed where ERA-Interim and HadGEM2-ES model outputs have been used to drive WRF. HadGEM2-ES is the Earth system model of the UK Met Office Hadley centre (Collins et al. 2011). The horizontal resolution of the atmospheric component is 1.875° by 1.25° with 38 vertical levels. The resolution of the ocean model is 1° by 1°, increasing to 1/3° at the equator, with 40 depth levels. HadGEM2-ES includes an interactive land and ocean carbon cycle as well as a dynamic vegetation model. An interactive tropospheric chemistry scheme is also included, which simulates the evolution of atmospheric composition and interactions with atmospheric aerosols. The model time step is 30 min for the atmosphere and land sub models and 1 h for the ocean sub model, with coupling between the atmosphere and the ocean every 24 h (Bellouin et al. 2011). The radiation transfer is computed at 3-hour intervals. More details of the model can be found in Johns et al. (2006) and Collins et al. (2011). The data for this study was produced with the atmosphere-only configuration of HadGEM2-ES with sea surface temperatures (SSTs) and sea ice cover (SIC) prescribed as surface boundary conditions. SSTs and SIC was provided by the bicentennial transient simulation (RCP4.5 scenarios) with HadGEM2-ES that has been conducted for CMIP5 (Collins et al. 2011).

The WRF model (Skamarock et al. 2008) is a non-hydrostatic model, suitable for simulating a wide range of scales, from thousands of kilometres to a few meters, with a large number of available options to configure the dynamical core and physical parameterisations, making it appropriate for numerical prediction. The choice of physical parameterization schemes is essential for obtaining better accuracy in climate downscaling experiments. We have conducted a series of sensitivity experiments with cumulus convection, land surface, cloud microphysics and boundary layer schemes to achieve an optimized configuration (Table 1) for downscaling experiment.

In this study initial and lateral boundary conditions from ERA-Interim and HadGEM2 global model have been used to drive the WRF model. The downscaling covered the geographical domain of Asia (-20 - 59 °N, 39 - 166 °E) with a horizontal resolution of 54 km and 36 vertical levels. The model domain and configuration used in this work are shown in Fig.1 and Table 1 respectively. The regional WRF model analysis is based on 40 years of HadGEM2-ES global model outputs spanning the periods of 1995-2005, 2015-2025, 2025-2035 and 2045-2055. These periods are labelled as 2000, 2020, 2030, 2050 as 'representing' the decadal climatologies used as boundary conditions for the WRF model to predict mean meteorological parameters on higher spatial resolution for future extreme events over south Asia. Further it's important to mention here that both the driving GCM and the RCM used in the study are stand-alone atmospheric models. The stand-alone AGCM and RCM may exaggerate the ocean forcing to atmosphere and lead to bias in climate projection over the Asian region (Zou et al. 2016, Wang et al. 2006).

To evaluate the model results, ERA-Interim reanalysis (hereafter referred to as ERA-Int; Dee et al. 2011) data has been used. The dataset is publicly available and can be obtained via http://apps.ecmwf.int/datasets/data/interim-full-daily/.

2.2 Analysis methodology

To quantify the changes in projected weather conditions, a range or predicted meteorological variables have been analysed. These include daily precipitation (Pr), 2-m mean, minimum and maximum temperature (Tmean, Tmin and Tmax), 10-m wind and horizontal components (W10, U10 and V10), mean sea level pressure (MSLP) and potential vorticity (PV) were used.

Empirical Orthogonal Functions (EOFs) have been calculated to identify possible dominant spatial modes of circulation patterns that explain the major variabilities in the model predictions. Our EOF analysis is based on the work of Kar et al. 2014; Hannachi et al. 2007; Wilks 1995. Climate indices shown in Table 2 were used for analysing extreme events (Klein et al. 2009; Zhang et al. 2011). A number of commonly used statistical metrics, such as Bias, Mean Absolute Error (MAE), and Mean Absolute Percentage Error (MAPE), were used for evaluation of model performance (see e.g. Wilks 1995). The analysis is conducted for the whole Asian domain and six sub regions, namely Central Asia (CA), East Asia (EA), North Asia (NA), South Asia (SA), South East Asia (SAE) and the Tibetan Plateau (TIB). The results are summarized in Table 3. The mathematical expressions used for different statistical metrics for model evaluation are given below:

$$Bias = \frac{1}{N}\sum_{k=1}^{N} p_k - o_k \tag{1}$$

$$Bias\% = \frac{BIAS}{\sum_{k=1}^{N} o_k} \tag{2}$$

$$MAE = \frac{1}{N}\sum_{k=1}^{N}|p_k - o_k| \tag{3}$$

$$MAPE = \frac{MAE}{\sum_{k=1}^{N} o_k} \tag{4}$$

where p_k stands for each individual predicted value, o_k for the observations and N the total number of predicted/observed values.

3. Results and discussions

In order to assess the confidence in the modelling approach, a detailed analysis of the model output using various skill metrics for the year 2000 is presented in this section. Further, the effects of regional meteorological conditions and atmospheric circulation on weather extremes over Asia and the sub regions are discussed.

3.1 Model evaluation

Figure 2 shows the observed and model simulated annual mean cycle of Tmax, Tmin and Pr over Asia. It can be seen from Figures 2a and 2b that for Tmax and Tmin, the model shows good agreement with observation, while it underestimates the precipitation by about 3 mm during summer (Fig. 2c). Further analysis shows an overall good agreement between observation and model simulation for most of the seasons (figure not shown). Looking at the sub-region level (Fig.3), during summer and autumn period higher biases are observed over South Asia (SA) and South-East Asia (SEA) regions. Further over the Tibetan Plateau (TIB) and SA regions, higher MSLP biases are present during summer and autumn seasons when compared to the other regions. Overall, the analysis suggests that the model is able to capture the seasonal changes in temperature, precipitation, wind and pressure that define the region's meteorology reasonably well.

3.2 Regional Meteorology: present climate and future changes

This section discusses the results of the present study to relate the regional meteorology for present day conditions and its future changes to the extreme meteorological events predicted over the six sub regions. The analysis is presented in terms of the meteorological variables of temperature, precipitation, wind and pressure.

3.2.1 Temperature

The variation of temperature between winter months (DJF) and summer months (JJA) are well depicted (figure not shown) and the contrast between inland and ocean is very well marked.

7

The changes in temperature are evident when analysing surface temperature's annual mean cycle for the present and future climate over six sub regions of Asia (Fig.4 a & b). An increase of temperature is expected throughout the year, especially during northern hemispherical winters. Although the temperature increase is predicted to occur over the entire region, the increase in Tmin would be stronger in South Asia (SA) and Tmax in Central Asia (CA) region.

3.2.2 Precipitation

The current modelling analysis of the entire Asian region for 2000 shows that the average daily accumulated precipitation was around 18 to 20 mm in the months of April - May, July-August and November, and around 5 to 15 mm for the remaining months. Further, for future years the precipitation is expected to increase (3-5 mm) over the entire Asian region by 2050 (figure not shown). Examining subregion wise for year 2000 (Fig. 5), it is noticed that for the July – August period the precipitation over EA, SA and SEA ranges between 20-30 mm/day. For CA, NA and TIB regions, the wintertime precipitation ranges between 6-12 mm/day. Looking into the individual regions for future years, the precipitation is expected to increase by 4-7 mm over SA and SEA regions in 2050.

3.2.3 Surface pressure and wind

The weather over the Asian region is influenced by several circulation patterns. The Siberian and Northern Pacific high pressure centres, the Aleutian, Inter Tropical Convergence Zone (ITCZ) and the Indian Ocean low pressure centres are all important atmospheric features which influence the circulation over the Asia region. In our model simulations (Figure not shown) the respective wind intensity decreases (~1.5 m/s) by 2050, and this could lead to less advection of polar air into the region of interest. Predictions further show that the strong southwesterly airflow slightly decreases in the north of the Himalayas. Overall, the analysis shows that the wind pattern is

not expected to vary considerably between present day and 2050. The monthly averaged wind intensity, however, seems to decrease but not significantly. Further analysis to characterise and quantify the change in the circulation patterns is presented below (section in 3.3) using EOF analysis for each variable.

3.3 Predominant Circulation Patterns

In order to detect persistent circulation anomalies associated with atmospheric changes over the Asian region, the empirical orthogonal function (EOF) based on the temporal covariance matric are computed and presented in this section.

3.3.1 Spatial distribution

The analysis is conducted by focusing on the anomalous spatial patterns uncovered by each EOF, and how much of the aggregated yearly and seasonal atmospheric circulation can be explained by them in terms of their variance. Table 4 shows the percentage variance of the first 5 EOFs for the variables, geopotential height (Z), MSLP, Tmax, Tmin, W10 and PV.

According to Table 4, nearly 60 % of the yearly MSLP circulation pattern is explained by its 1st EOF, i.e., for most of half of the year. When analysing the seasonal results, it shows that the 1st EOF explains 38 - 43 % of the anomalous pattern for most of the seasons except for summer which accounts for only 19 %. More dominant effects are presented by the 1st EOF of Z followed by Tmax and Tmin that show an annual percentage of 80 to 82 % and a seasonal percentage ranging between 23 to 68 %. Fig.6 presents the winter's first EOFs regarding Z_{300}, Tmin, W10 and Pr. The 1st winter EOF of Z (Fig.6) exhibits a strong positive anomaly over upper parts of Asia. When analysing other variables such as Tmin and Tmax, they indicate a similar pattern, where 56% of winter temperature anomalies seem to follow the same persistent anomaly present in the geopotential height and the MSLP differences for this season. Further the 1st and 2nd mode for

wintertime wind circulation (Fig.6) is also showing a southerly flow towards South China which is responsible for exposing the region to milder temperatures. This feature is also seen in the 2nd EOF of Tmin where very low PV anomaly is present.

According to Kang et al. (1999) there are three important modes affecting the Asian summer which are discussed below. All the three modes are well depicted here by the first EOFs of MSLP, PV and W10. The first mode is associated with the annual cycle of the hemispheric monsoon characterised by a low-pressure system in the northern hemisphere from June to mid-August (Fig. 7). This mode is represented in the precipitation field with a very well pronounced dry region over oceanic and a wet region in SEA towards the north. A similar situation occurs for temperature and wind fields (Fig. 7) with a steep south-north gradient of anomalous temperatures and the inland wind anomaly on EOF1 of wind, bringing the moist air into the coastal regions of SA and EA as the South Asian Monsoon (SAM) and East Asian Monsoon (EAM) during the summer months.

The EOF oscillation becomes clearer once we examine the coefficient time series for these modes of persistent circulation patterns to which the respective synoptic conditions are influencing regional meteorology, especially with respect to extreme events (e.g. Herring et al. 2014; Houze et al. 2011). The next section (3.3.2) considers how these modes are likely to change in future years and how they will affect regional meteorology and extreme events.

3.3.2 Expected changes and its effects on regional meteorology

We investigated the coefficients of time series of EOFs over Asia and sub regions. Looking back at the Tmin for winter (section 3.1.1, Fig. 4), the increase of Tmin, especially over TIB and CA seem to reflect the positive anomalies from the 1st EOF. This increase becomes clear when analysing the coefficients just for the winter months depicted in Fig.8, where there is a clear

increase on the lower and upper limits until 2050. This mode accounts for half of the wintertime circulation (Table 4). Perturbations of the meridional and zonal winds also show an increase in variance, although not as prominent as the other variables. Nevertheless, in the upper regions of the troposphere at 300hPa an increase of the negative PV anomaly over TIB and CA region can be associated with the anti-cyclonic anomaly depicted in the $(U, V)_{300}$ field for the winter months (Fig.9a). Also present in the 10-m wind 1st EOF and 3rd EOF of PV (Fig.9b) is the southerly flow from SEA into coastal China all the way to the South Korean coast that seems to intensify until 2050 to bring moist and milder weather into the EA, CA and TIB region. An important feature that could be associated to the TIB region winter precipitation is the increased southerly flow from the Indian Ocean (SA region), along the Indian west coast into the TIB region (Fig.9c). As the southerly flow advects moisture, the probability of convection occurring is most likely over the region due to hindrance from the Himalayan orography. This is confirmed with the PV, 1st and 3rd EOF (Fig.9a &b), where strong positive anomalies associated with horizontal convergence and convection, are found over the region, thus influencing the precipitation. This milder and moister weather intrusion from both these anomalies seems to be in line with the positive temperature anomalies and the precipitation maxima over TIB, EA and CA as mentioned earlier. The overall pattern over Asia is influenced by anti-cyclonic anomaly and low PV anomalies as seen by the 1st EOF, implies that less favourable conditions for convective episodes are likely to increase. This could have an impact on cold waves, cold spells and winter droughts in the most affected regions. Further, since the 1st and 2nd EOFs are related with the monsoonal activity, i.e., SAM, EAM, and SEAM respectively, we have investigated the temporal amplitudes of Z_{300}, W10, PV_{300} and Pr depicted in Fig.10. Negative anomalies for Z_{300} are in phase with the strengthening of the wind anomaly intensity for all the three monsoon systems over EA, SA and SEA. These anomalies seem

11

to decrease in 2020 and 2030 where the negative limit for the EOF coefficient becomes less negative regarding EAM and SAM. Wind coefficients show an increasing trend of negative amplitudes and suggest a weakening of the monsoonal circulation.

While the mean and anomalous regional meteorology and circulation and its future changes have been presented, the weather extremes for the present and future years are discussed below in the context of regional circulation analysis.

3.4 Climate Variability and Weather Extremes

There is general agreement that changes in the frequency or intensity of extreme weather and climate events would have profound impacts on both human society and the natural environment (IPCC AR5). In this section, the spatial and temporal study of weather extremes, their expected changes and how they are connected with predominant circulation patterns is discussed. Temperature extremes (heat waves, warm spells, cold spells and cold waves), precipitation extremes (such as heavy precipitation above a certain daily threshold, droughts and wet periods) and wind extremes (such as strong breeze days and strong wind days) have been analysed.

3.4.1 Evolution of extremes: frequency and duration

3.4.1.1 Heat waves and cold waves

The predicted number of heat waves (HW) and duration days for Asia are shown in Fig. 11. It can be noticed from the diagram that there is an increase in both number and duration of heat waves over SA and EA regions by 2050. For e.g. over the SA region the heat wave duration is up to 50 days with most of region being affected by up to 5 days and about 10% being affected by up to 35 days. For the summer season, the upper range value from the modelling analysis implies that about half of the season will be under influence of heat wave by 2050. Examining the warm spells, although the number of spells and their duration in days is not increasing, the spatial distribution is

increasing from 20-40 % (Fig.12a & b). This implies that from periods of 2020 to 2050 more than 25% of the region will be affected by temperature extreme. Furthermore, during wintertime, the CA region is affected by 1-3 cold waves in each winter as seen in Fig.13. More than 60 % of the region will be under the influence of at least one cold wave until 2050, whereas up to 20% of the region will be influenced by more, although it's decreasing until 2050. Similar analysis for NA, SA, TIB and EA region conducted (for the sake of brevity figure not shown), and its seen that cold spell seem to follow the same frequency and duration trend for 2050 compared to present.

3.4.1.2 Droughts, wet periods and heavy precipitation

In Fig. 14, the analysis shows that the CA region will experience an increase in consecutive dry days during summer and a decrease in number of wet days over a lesser percentage area, i.e., more frequent events are likely to affect smaller areas. Further, analysing EA region shown in Fig.14, consecutive wet days show a slight increase (~4%) until 2050 for the 5 consecutive days, although its spatial coverage will decrease with the increase of the frequency of the wet days. The trend in heavy precipitation follows the same spatial and temporal pattern and the high frequency of dry days are expected to decrease with a lesser spatial extension. The differences between northern and southern regions can be explained since southern regions are under the influence of the EAM and SAM. Furthermore, simulation shows that with respect to droughts and heavy precipitation, summertime extremes will be more spatially heterogeneous compared to wintertime extremes. Analysis of all regions showed similar patterns, a decrease of wintertime frequency of wet days accompanied by an increase in dry day's frequency until 2050 (Figure not shown).

3.4.1.3 Strong breeze events

To examine seasonal wind extremes, summer and winter frequencies and spatial distributions have been analysed and are shown in Fig.15. It can be noticed from the figure that in

both seasons, the spatial coverage decreases with the increase in frequency of days. Looking at the EA and SA regions, most of the EA strong breeze days are concentrated between 5 to 25 consecutive days during summer, while in the SA there seems to be more consecutive strong breeze days throughout the season. Also, the spatial coverage seems to decrease until 2050 on 5 consecutive days in EA, but it is increasing in SA. This is due to different wind regimes and different monsoonal dynamics (Webster et al. 1998) during summertime. During winter, both distributions are similar for EA and SA. TIB and CA are likely to have more frequent days of strong winds during winter although spatial coverage decreases, i.e., small portions of land are under continuous strong wind days during winter. To be noticed that TIB shows a greater spatial coverage throughout the consecutive days in winter time, most likely because of the predominance of complex terrain circulation over the region.

3.4.2 Association of high weather extremes with predominant circulation patterns

During summer, predominant circulation patterns showed positive anomalies in temperature over areas in SA, SEA, NA and EA. Moreover, the negative PV anomalies associated indicate horizontal divergence, i.e., increased stratification and hence, more stable conditions. These are in line with the increase of the number of heat waves and severe droughts over these regions with time as discussed in section 3.4.1.1. Furthermore, a stronger cyclonic anomaly over Asia with positive PV anomaly over EA can also be a precursor of the increase in wet days and 5-day period of consecutive wet days in EA during early summer in 2050. Positive PV anomalies are related with horizontal convergence, and, if there is a considerable amount of moisture in the atmosphere, convection is possible increasing the likelihood of more advection of the moist air from the Pacific Ocean during EAM. In terms of the changes expected during future winder seasons by 2050, the decrease of precipitation can be explained by the persistency of anti-cyclonic anomalies associated

with negative PV anomalies and hence horizontal divergence where precipitation is less likely to occur, giving rise to increasing atmospheric stability and droughts events.

4. Conclusion

A dynamical modelling framework based on HadGEM2-ES and WRF models has been used to undertake a comprehensive study of the role of regional meteorology and circulation patterns on extreme events over Asia for the present and future years. Four representative periods, based on 40 years of HadGEM2-ES global model outputs were considered for the WRF regional model analysis. The key findings of the study are summarized as follows:

(i) While there are some systematic biases present as compared to the observations, overall, the model simulations (for the period 2000) are able to delineate the observed features of temperature, winds, precipitation and pressure over region of interest reasonably well.

(ii) There is an overall increase in wintertime minimum temperature by 3-4^{0}C over the entire Asian domain, however, the increase in Tmin is stronger in SA and CA region. Summer precipitation increases by 4-7 mm/day over SA and SEA region by 2050. Further this study indicates that wind pattern are unlikely to vary considerably until 2050 but the monthly averaged wind intensity is expected to decrease slightly. In particular, this is likely for the north - easterly flows due to the gradient between the Siberian High and the Aleutian Low.

(iii) When examining regional circulation and extremes under the global warming scenario, anti-cyclonic activity associated with low PV anomalies and high positive temperature anomalies during late summer influences the increase in frequency (3-4) and duration (about 30 days) of heat waves and severe droughts over SA, SEA, EA and NA. A strong cyclonic anomaly and positive PV anomaly over EA in early summers may influence the increase of consecutive wet days as the air is carrying moisture from EAM circulation, and convection is possible under

favourable conditions. During wintertime, a more pronounced anti-cyclonic anomaly along with low PV anomaly is predicted to favour the conditions for less precipitation as the stratification will increase until 2050 leading to more stable atmospheric conditions.

This study provides important insight into how weather conditions will change in the future over Asia. Results of this study will have major implications for environmental, health and socioeconomic state of the region especially during periods of drought, heat waves and changing precipitation patterns. However, its worth mentioning here that both GCM and RCM used in the present work are stand-alone models and hence a fully coupled model simulations are needed for projections of Asian climate. We recommended that an international fully coupled high resolution multi-model exercise focussing on extreme events will provide further understanding and corroboration of the conclusion of this study by examining not only the impacts for the south Asia region but also for other regions of the world.

Contributions

All authors collaborated in the research presented in this publication by making the following contributions: research conceptualization, Ranjeet S. Sokhi (RSS), P. R. Tiwari (PRT), Joanna S.N. de Medeiros (JM), Gerd A. Folberth (GAF) and William J. Collins (WJC); methodology, RSS, PRT and JM; formal analysis, JM; writing—original draft preparation, RSS, JM, PRT; writing—review and editing, RSS, GAF, and WJC; supervision, RSS and PRT.

Declarations

Availability of data and material: The data and material used in this research will be available upon request from the corresponding author.

Code availability: Available upon request from the corresponding author.

Ethics approval

This study did not involve any protected area, private land, and endangered or protected species. And no specific permissions were required for this activity.

Consent to participate

Not applicable.

Consent for publication

Written informed consent for publication was obtained from all authors.

Conflict of interest

The authors declare that they have no conflict of interest.

References

Andrade C, Leite SM, Santos JA (2012) Temperature extremes in Europe: overview of their driving atmospheric patterns. Nat Hazard Earth Sys 12: 1671-1691.

Barriopedro D, Fischer EM, Luterbacher J, Trigo RM, García-Herrera R (2011) The hot summer of 2010: Redrawing the temperature record map of Europe. Science 332: 220–224.

Bellouin N, Rae J, Jones A, Johnson C, Haywood J, Boucher O (2011) Aerosol forcing in the Climate Model Intercomparison Project (CMIP5) simulations by HadGEM2-ES and the role of ammonium nitrate. J Geophys Res 116, D20206, doi:10.1029/2011JD016074.

Buehler T, Raible CC, Stocker TF (2011) The relationship of winter season North Atlantic blocking frequencies to extreme cold or dry spells in the ERA-40. Tellus 63: 212–222.

Cassou C, Terray L, Phillips AS (2005) Tropical Atlantic influence on European heat waves. J Climate 18: 2805–2811.

Chen Y, Zhai P (2013) Persistent extreme precipitation events in China during 1951–2010. Clim Res 57: 143–155.

Collins WJ, Bellouin N, Doutriaux-Boucher M, Gedney N, Halloran P, Hinton T, Hughes J, Jones CD, Joshi M, Liddicoat S, Martin G, O'Connor F, Rae J, Senior C, Sitch S, Totterdell I, Wiltshire A, Woodward S (2011) Development and evaluation of an Earth-System model – HadGEM2. Geosci Model Dev 4: 1051–1075.

Dee DP, Coauthors (2011) The ERA-Interim reanalysis: Configuration and performance of the data assimilation system. Q J R Meteorol Soc 137: 553–597.

Della-Marta PM, Haylock MR, Luterbacher J, Wanner H (2007) Doubled length of western European heat waves since 1880. J Geophys Res 112: D15103. doi:10.1029/2007JD008510.

Dole R, Hoerling M, Perlwitz J, Eischeid J, Pegion P, Zhang T, Quan XW, Xu T, Murray D (2011) Was there a basis for anticipating the 2010 Russian heat wave? Geophys Res Lett 38: L06702, doi:10.1029/2010GL046582.

Dileepkumar R, AchutaRao K, Arulalan T (2018) Human influence on sub-regional surface air temperature change over India. Sci Rep 8: 8967.

Flato G, Marotzke J, Abiodun B, Braconnot P, Chou SC, Collins W, Cox P, Driouech F, Emori S, Eyring V, Forest C, Gleckler P, Guilyardi E, Jakob C, Kattsov V, Reason C, Rummukainen M (2013) Evaluation of climate models. In Climate Change 2013: The Physical Science Basis. Contribution of Working Group I to the Fifth Assessment Report of the Intergovernmental Panel on Climate Change. [StockeR TF, Qin D, Plattner GK, Tignor M, Allen SK, Boschung J, Nauels A, Xia Y, Bex V, Midgley PM *Eds*. Cambridge University Press 741-882, doi: 10.1017/CBO9781107415324.020.

Gu H, Wang G, Yu Z, Mei R (2012) Assessing future climate changes and extreme indicators in east and south Asia using RegCM regional climate model. Clim Chang 114: 301–317.

Hannachi A, Joliffe I, Stephenson D (2007) Empirical orthogonal functions and related techniques in atmospheric science: A review. Int J Climatol 27: 1119–1152.

Herring SC, Hoerling MP, Peterson TC, Stott PA (2014) Explaining extreme events of 2013 from a climate perspective. Bull Amer Meteor Soc 95: S1–S96, doi: 10.1175/1520-0477-95.9.S1.1.

Houze RAJR, Rasmussen KL, Medina S, Brodzik SR, Romatschke U (2011) Anomalous atmospheric events leading to the summer 2010 floods in Pakistan. Bull Amer Meteor Soc 92: 291–298, doi: 10.1175/2010BAMS3173.1.

Johns TC, Coauthors (2006) The new Hadley Centre climate model HadGEM1: Evaluation of coupled simulations. J Climate 19: 1327–1353.

Kang I S, Ho CH, Lim YK, Lau KM (1999) Principal modes of climatological seasonal and intraseasonal variations of the Asian summer monsoon. Mon Weath Rev 127: 322–339.

Kar SC, Rana S (2014) Interannual variability of winter precipitation over northwest India and adjoining region: impact of global forcings. Theor Appl Climatol doi: 10.1007/s00704-013-0968-z.

Klein AMG, Zwiers FW, Zhang X (2009) Guidelines on analysis of extremes in a changing climate in support of informed decisions for adaptation. Climate data and monitoring. WCDMP-No. 72, WMO-TD No. 1500, pp. 56.

Kumar A, Jimenez R, Belalcazar LC, Rojas N (2015) Application of WRF-Chem Model to Simulate PM10 Concentration over Bogota. Aerosol and Air Quality Res. 16(5): doi: 10.4209/aaqr.2015.05.0318.

Li D, Zhou T, Zhang W (2019) Extreme precipitation over East Asia under 1.5 °C and 2 °C global warming targets: a comparison of stabilized and overshoot projections. Environ Res Commun https://doi.org/10.1088/2515-7620/ab3971.

Ma S, Zhou T, Angelil O, Shiogama H (2017a) Increased Chances of Drought in Southeastern Periphery of the Tibetan Plateau Induced by Anthropogenic Warming. J Clim 30: 6543-6560.

Ma S, Zhou T, Stone D, Angelil O, Shiogama H (2017b) Attribution of the July-August 2013 Heat Event in Central and Eastern China to Anthropogenic Greenhouse Gas Emissions. Environ Res Lett 12: 054020.

Maharana P, Dimri AP, Choudhary A (2020) Future changes in Indian summer monsoon characteristics under 1.5 and 2 °C specific warming levels. Clim Dyn 54: 507–523.

Panda SK, Dash SK, Bhaskaran B, Pattnayak KC (2016) Investigation of the snow-monsoon relationship in a warming atmosphere using Hadley Center climate model. Glob Planet Chang 147:125–136.

Pattnayak KC, Panda SK, Saraswat V, Dash SK (2016) Relationship between tropospheric temperature and Indian summer monsoon rainfall as simulated by RegCM3. Clim Dyn 46(9–10): 3149–3162.

Rohini P, Rajeevan M, Srivastava A (2016) On the Variability and Increasing Trends of Heat Waves over India. Sci Rep 6: 26153. https://doi.org/10.1038/srep26153.

Santos J, Corte-Real J (2006) Temperature extremes in Europe and wintertime large-scale atmospheric circulation: HadCM3 future scenarios. Clim Res 31: 3-18.

Skamarock WC, Klemp JB, Dudhia J, Gill D, Barker D, Duda M, Huang H, Wang W, Powers JG (2008) A description of the Advanced Research WRF Version 3. NCAR Technical Note NCAR/TN-475+STR.

Sillmann J, Croci-Maspoli M, Kallache M, Katz RW (2011) Extreme cold winter temperatures in Europe under the influence of North Atlantic atmospheric blocking. J Clim 24: 5899–5913.

Tiwari PR, Kar, SC, Mohanty, UC, Dey S, Sinha P, Shekhar MS (2017) Sensitivity of the Himalayan orography representation in simulation of winter precipitation using Regional Climate Model (RegCM) nested in a GCM. Clim Dyn 49: 4157–4170.

Trenberth KE, Dai A, Rasmussen RM, Parsons DB (2003) The changing character of precipitation. Bull Amer Meteor Soc 84: 1205–1217.

Trigo IF (2006) Climatology and interannual variability of stormtracks in the Euro-Atlantic sector: a comparison between ERA-40 and NCEP/NCAR reanalysis. Clim Dyn 26: 127–143.

Ulbrich U, Brücher T, Fink AH, Leckebusch GC, Krüger A, Pinto JG (2003) The central European floods in August 2002. Part II: synoptic causes and considerations with respect to climate change. Weather 58: 434–442.

Wang B, Ding Q, Fu X, Kang IS, Jin K, Shukla J, Doblas-Reyes F (2005) Fundamental challenge in simulation and prediction of summer monsoon rainfall, Geophy Res Lett 32:L15711, doi:10.1029/2005GL022734.

Webster PJ, Magaña VO, Palmer TN, Shukla J, Tomas RA, Yanai M, Yasunari T (1998) Monsoons: Processes, predictability, and the prospects for prediction. J Geophys Res 103(C7): 14451–14510.

Wilks DS (1995) Statistical Methods in the Atmospheric Sciences. Academic Press, 467 pp.

Yiou P, Nogaj M (2004) Extreme climatic events and weather regimes over the North Atlantic: When and where? Geophys Res Lett **31**: L07202, doi:10.1029/2003GL019119.

Zhang L, Wu P, Zhou T, Xiao C (2018) ENSO Transition from La Nina to El Nino Drives Prolonged Spring-Summer Drought over North China. J Climate 31: 3509-3523.

Zhang L, Wu P, Zhou T (2017) Aerosol Forcing of Extreme Summer Drought over North China. Environ Res Letters 12 (3): 034020.

Zhang X, Alexander LV, Hegerl GC, Jones P, Klein Tank AMG, Peterson TC, Trewin B, Zwiers FW (2011) Indices for monitoring changes in extremes based on daily temperature and precipitation data. Wiley Interdiscip Rev: Clim Chang 2: 851–870.

Zou L, Zhou T, Peng, D (2016) Dynamical downscaling of historical climate over CORDEX East Asia domain: a comparison of regional ocean atmosphere coupled model to standalone RCM simulations. J Geophy Res Atmos 121:1442–1458. doi:10.1002/2015JD023912.

List of Figures

Figure 1: WRF model domain and topography (in m) considered in the study.

Figure 2: Annual mean cycle for Asia regarding: a) Tmax, b) Tmin and c) Pr for WRF (black) and ERA-I (red).

Figure 3: Bias for each region for: a) Tmax, b) Tmin, c) Pr, d) U10, e) V10, f) W10 and g) MSLP. Regions are NA, CA, TIB, EA, SA and SEA respectively.

Figure 4: a) Tmin mean annual cycle (2000, 2020, 2030 and 2050) for the six regions: NA, CA, TIB, EA, SA and SEA; b) same as of figure a) but for Tmax.

Figure 5: Annual precipitation cycle (2000, 2020, 2030 and 2050) for the six regions: NA, CA, TIB, EA, SA and SEA.

Figure 6: First three winter EOFs (top to bottom) regarding Z_{300}, Tmin, W10 and Pr.

Figure 7: Summer EOFs 1, 2 and 4 (left to right) for MSLP, W10, PV(U,V) at 300 hPa and Pr.

Figure 8: EOF1 coefficients for Tmin for the entire years (top) and winter months only (bottom) regarding Asia, TIB and CA (from left to right).

Figure 9: a) EOF1 and series coefficients for PV_{300} for winter months regarding Asia, CA, TIB and NA (from left to right); b) PV_{300} EOF3 and series coefficients for Pr for winter months regarding Asia, CA, TIB and EA (from left to right) and c) W10 EOF1 and series coefficients for V10 for winter months regarding Asia, CA, SA and SEA (from left to right).

Figure 10: EOF1 coefficients for Z300, W10, PV300 and Pr (top to bottom) regarding EA, SA regions and EOF2 regarding SEA region for the summer months, representing the Asian Monsoonal circulation.

Figure 11: a) Number of Heat Waves (HW) and b) duration days regarding the Asia regions of NA, CA and SA for 2020 (blue), 2030 (cyan) and 2050 (yellow) during summer months.

Figure 12: a) Number of warm spells and b) duration days regarding the Asia regions of NA, CA and SA for 2020 (blue), 2030 (cyan) and 2050 (yellow) during summer months.

Figure 13: a) Number of Cold Waves (CW) regarding the Asia regions of NA, CA and TIB for 2020 (blue), 2030 (cyan) and 2050 (yellow); and b) duration days for the entire region during winter months.

Figure 14: Number of cdd and cwd for the Asia regions of NA, CA, TIB, EA, SA, SEA for 2020 (blue), 2030 (cyan) and 2050 (yellow) during the summer months.
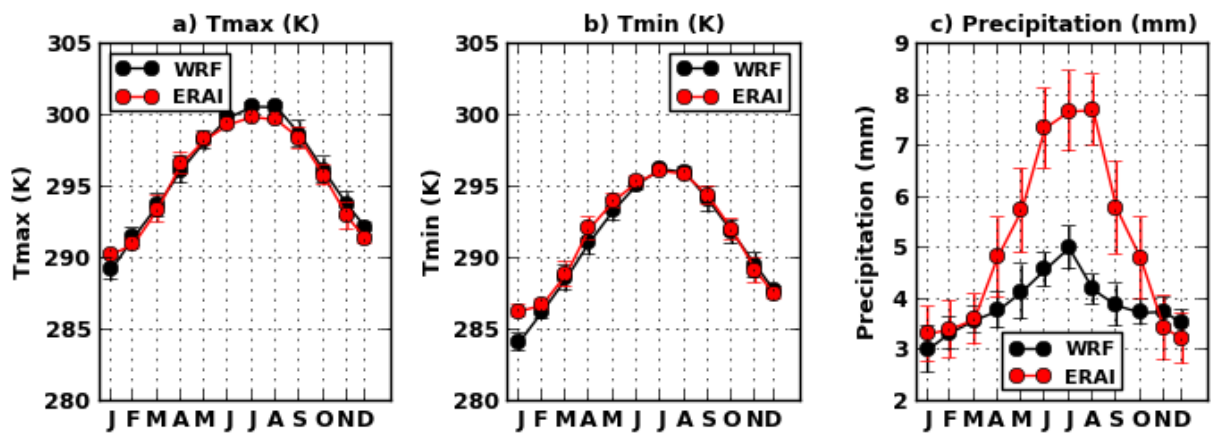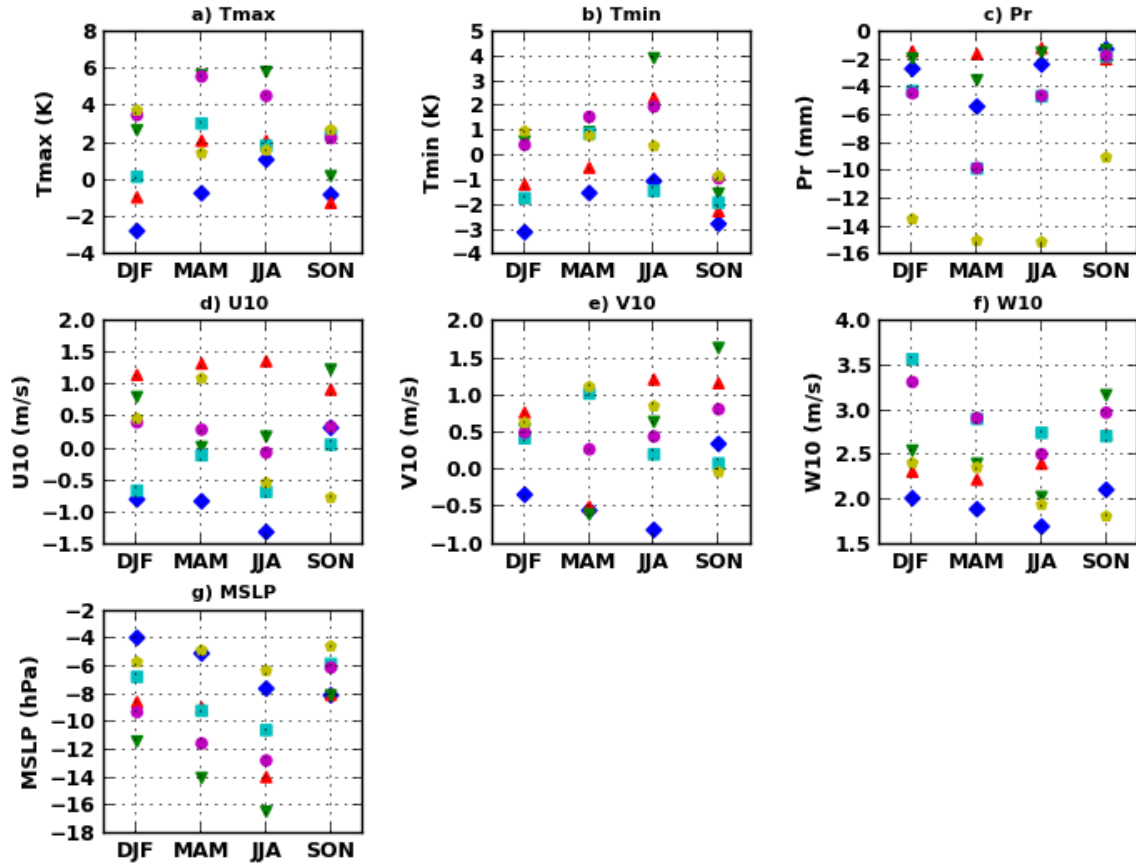
Figure 15: Number strbre for the Asia regions of CA, TIB, EA and SA for 2020 (blue), 2030 (cyan) and 2050 (yellow) during the summer and winter months.
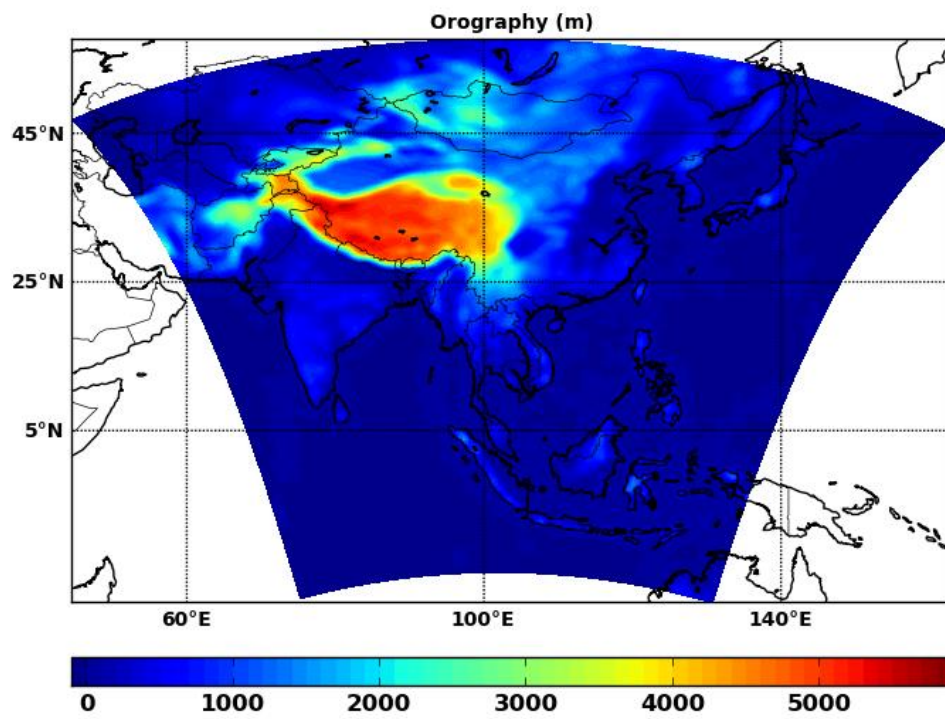
Figure 1. WRF topography (in m) and full WRF model domain considered in the study.

Figure 2. Annual mean cycle for Asia regarding: a) Tmax, b) Tmin and c) Pr for WRF (black) and ERA-Int (red).

Figure 3. Bias for each region for: a) Tmax, b) Tmin, c) Pr, d) U10, e) V10, f) W10 and g) MSLP. Regions are NA (blue), CA (red), TIB (green), EA (light blue), SA (purple) and SEA (yellow) respectively.

(a)
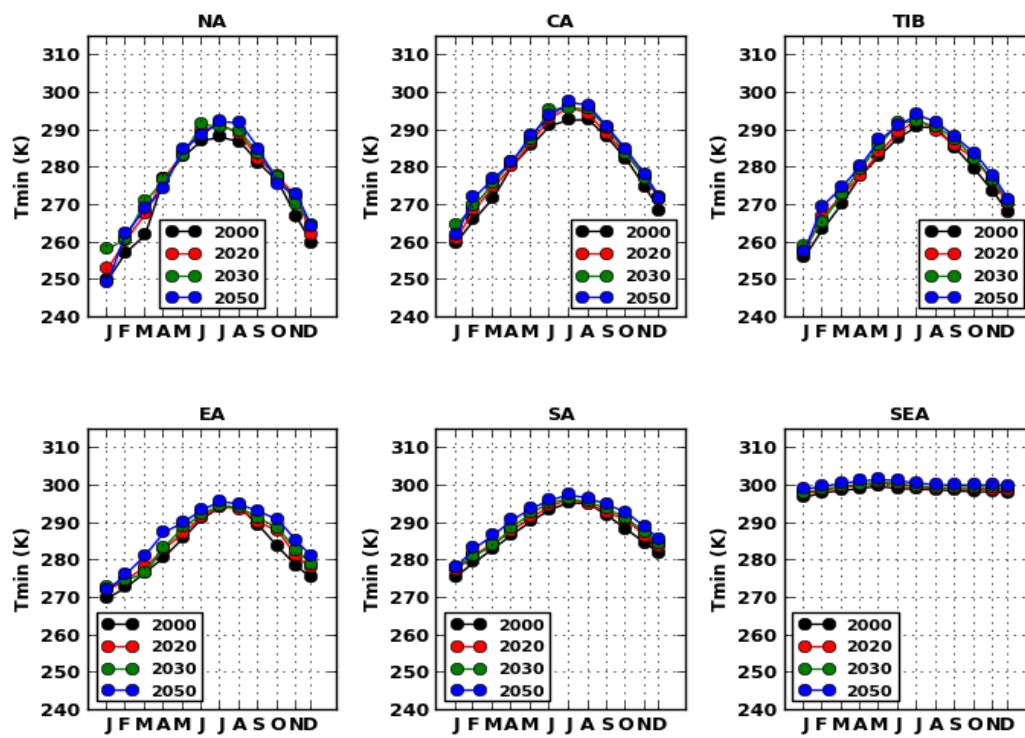
b)
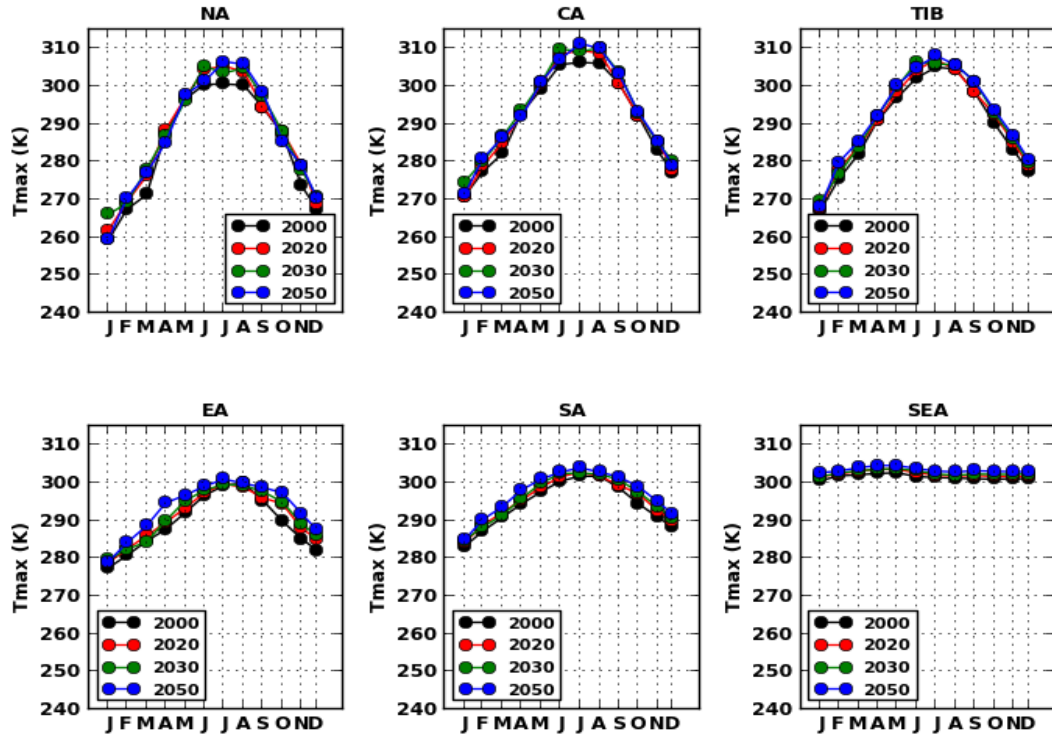
Figure 4. a) Tmin mean annual cycle (2000, 2020, 2030 and 2050) for the six regions: NA, CA, TIB, EA, SA and SEA; b) same as of figure a) but for Tmax.
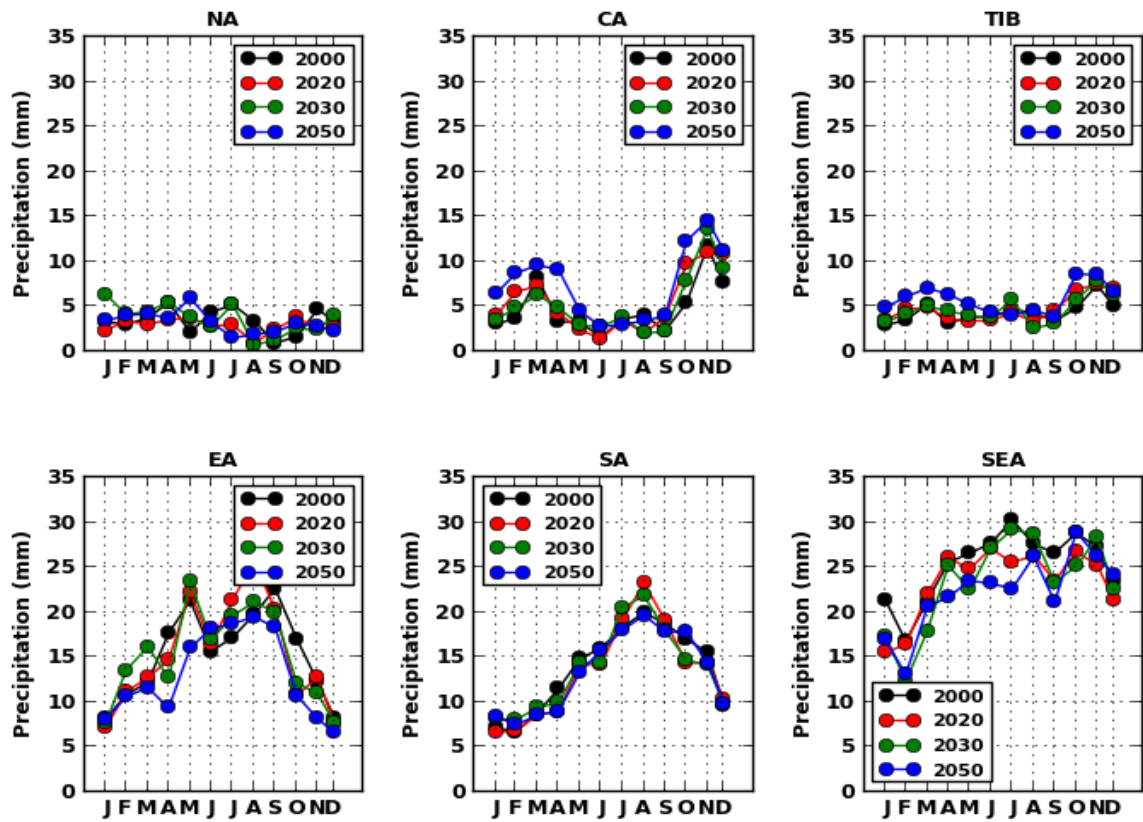
Figure 5. Annual precipitation cycle (2000, 2020, 2030 and 2050) for the six regions: NA, CA, TIB, EA, SA and SEA.
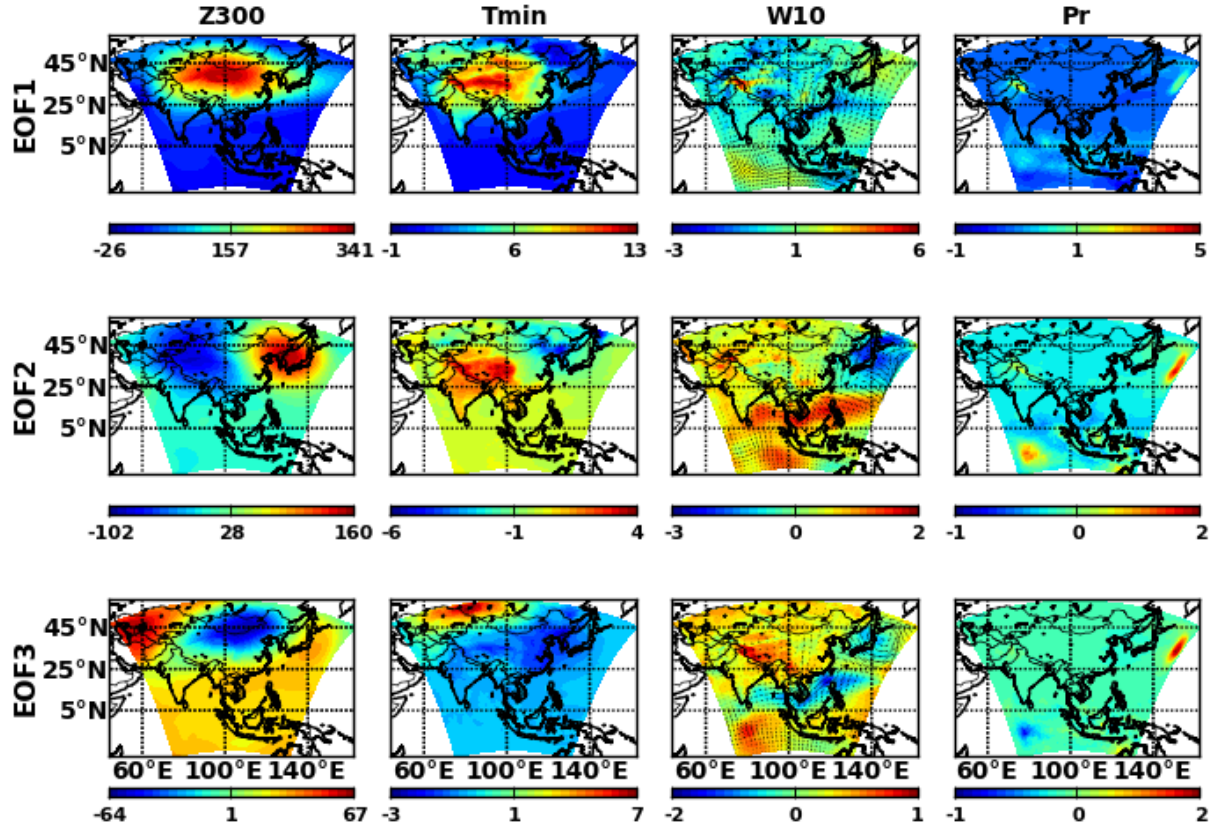
Figure 6. First three winter EOFs (top to bottom) regarding Z_{300}, Tmin, W10 and Pr.
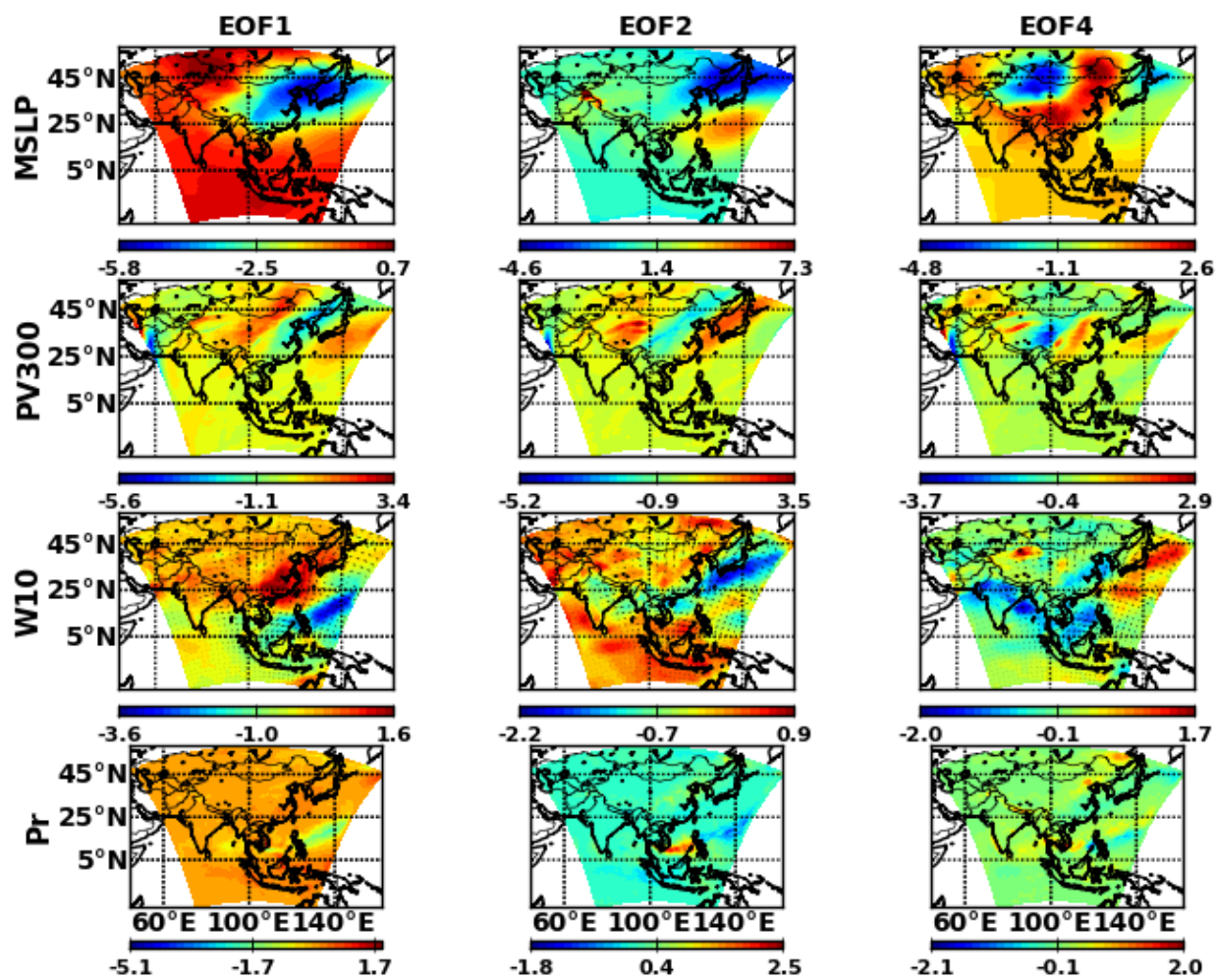
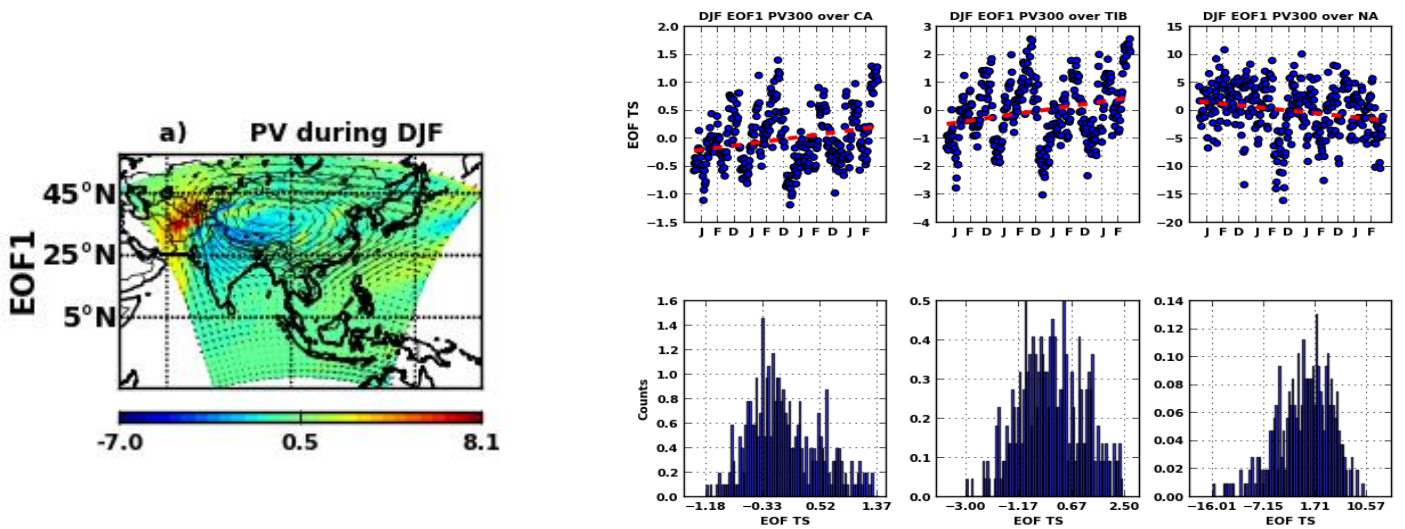Figure 7. Summer EOFs 1, 2 and 4 (left to right) for MSLP, W10, PV(U,V) at 300 hPa and Pr.
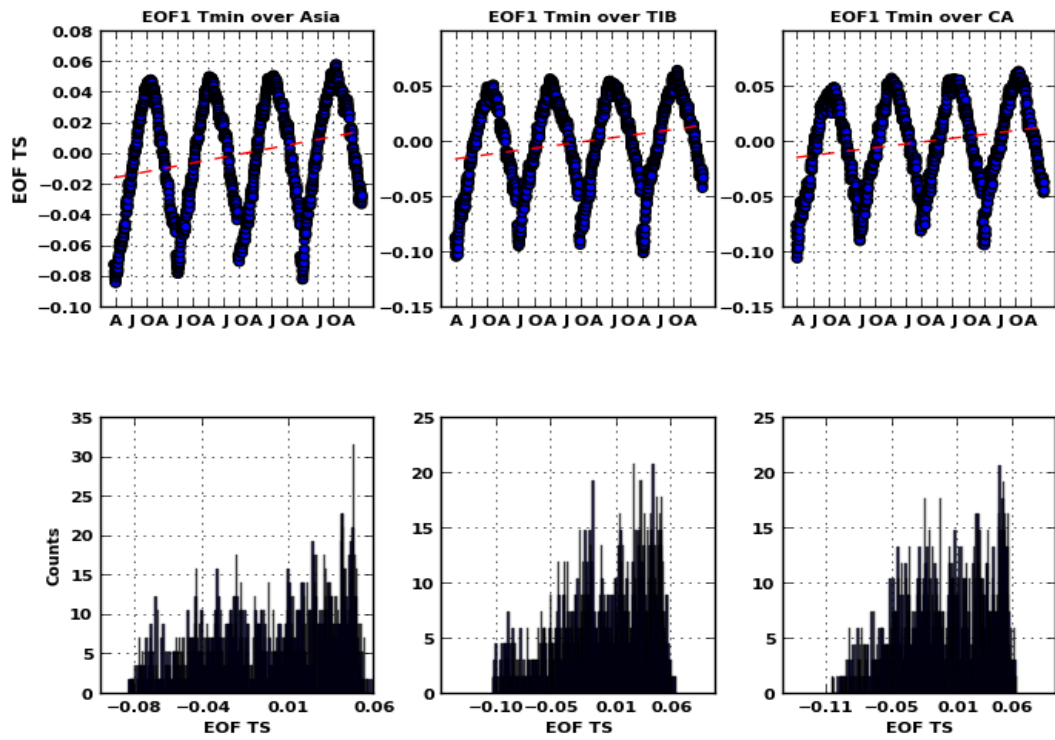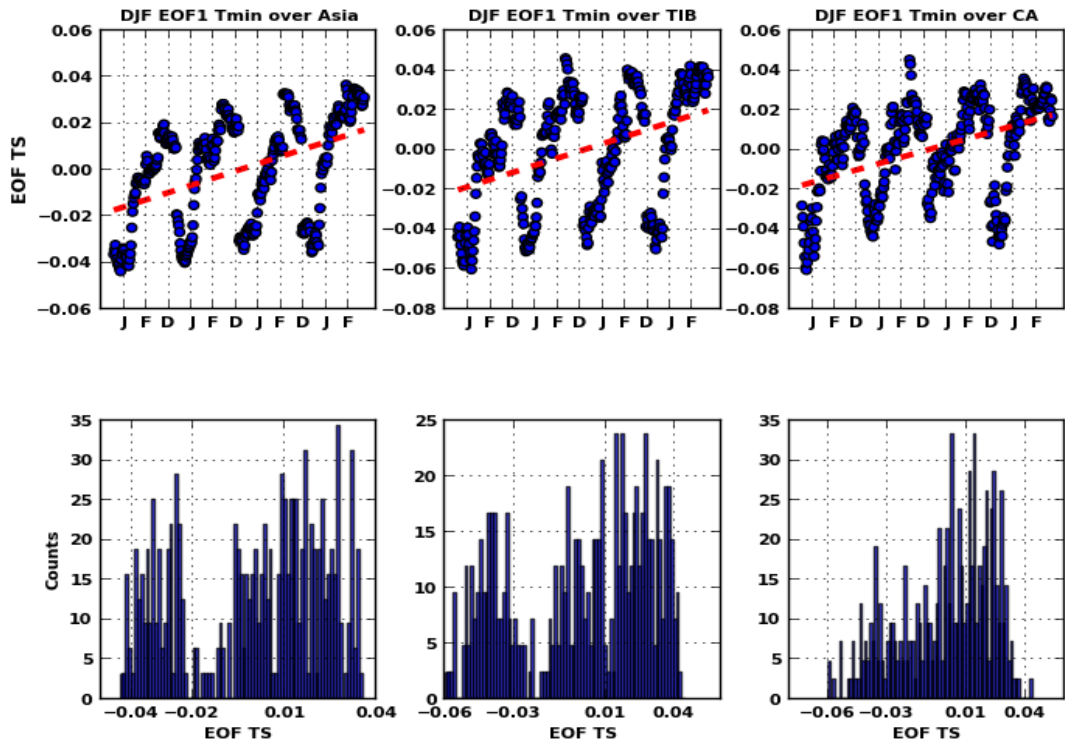
Figure 8. EOF1 coefficients for Tmin for the entire years 2000-2050 (top) and winter months only (bottom) regarding Asia, TIB and CA (from left to right).
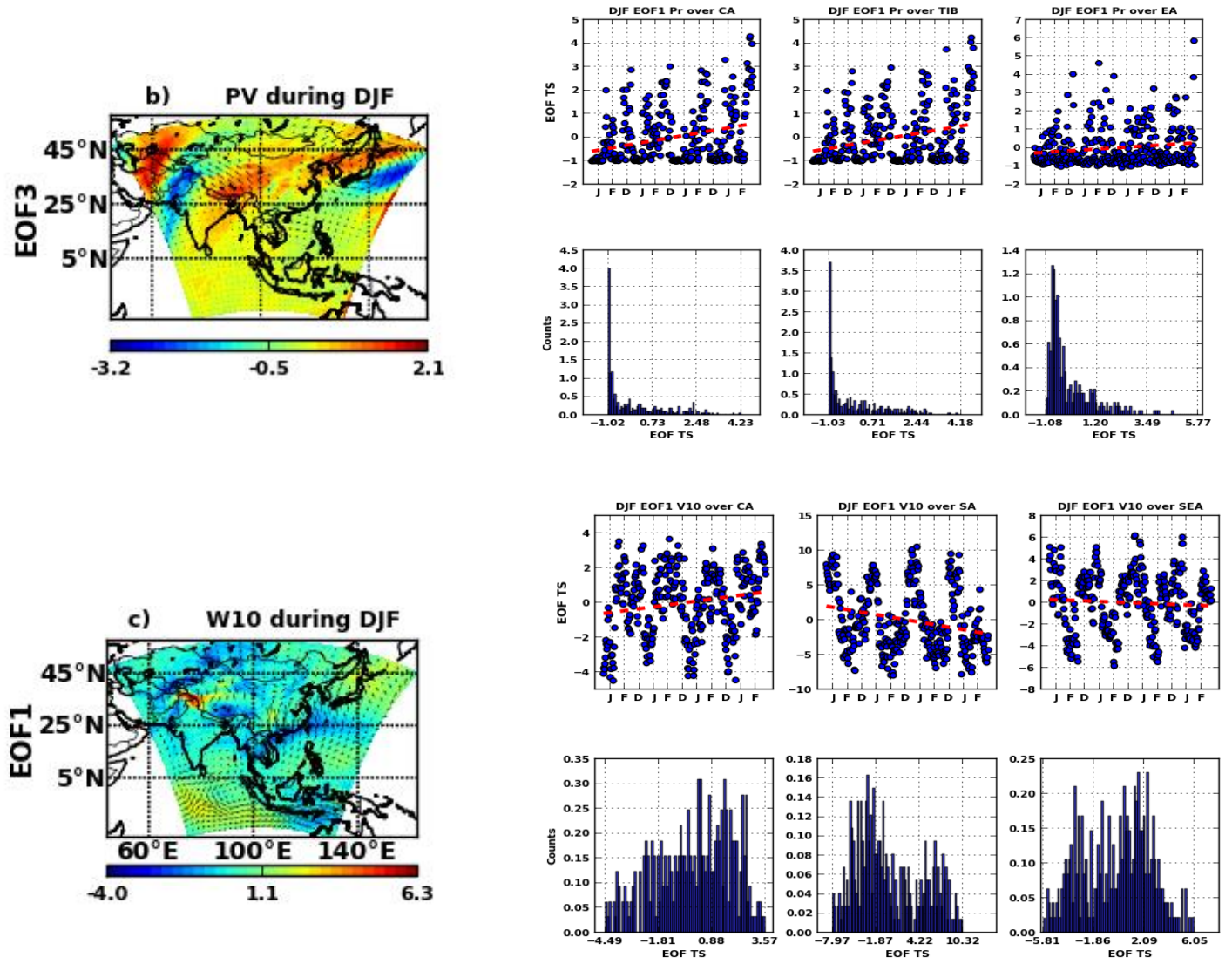
Figure 9. a) EOF1 and series coefficients for PV$_{300}$ for winter months regarding Asia, CA, TIB and NA (from left to right); b) PV$_{300}$ EOF3 and series coefficients for Pr for winter months regarding Asia, CA, TIB and EA (from left to right) and c) W10 EOF1 and series coefficients for V10 for winter months regarding Asia, CA, SA and SEA (from left to right).
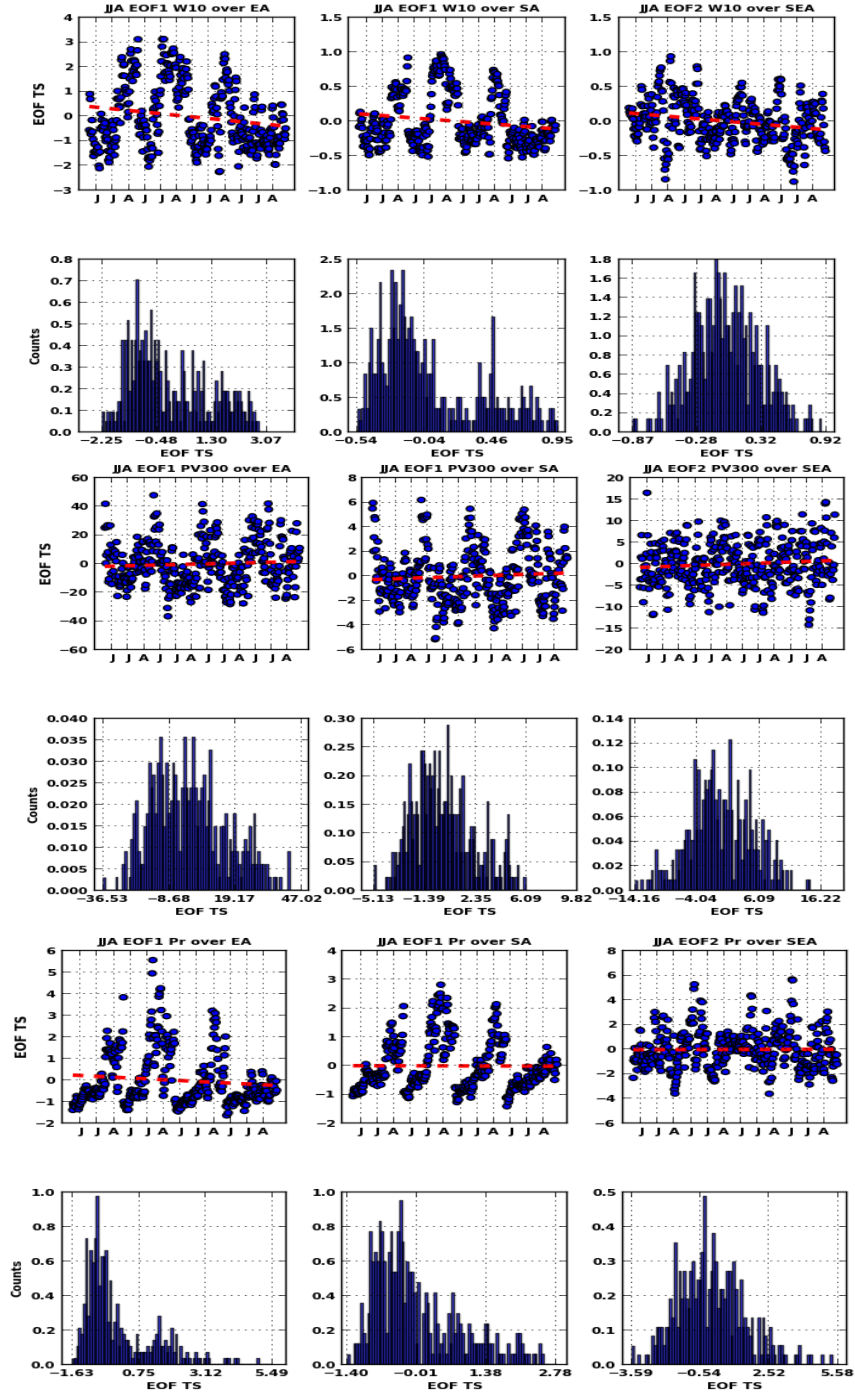
Figure 10. EOF1 coefficients for Z300, W10, PV300 and Pr (top to bottom) regarding EA, SA regions and EOF2 regarding SEA region for the summer months, representing the Asian Monsoonal circulation.
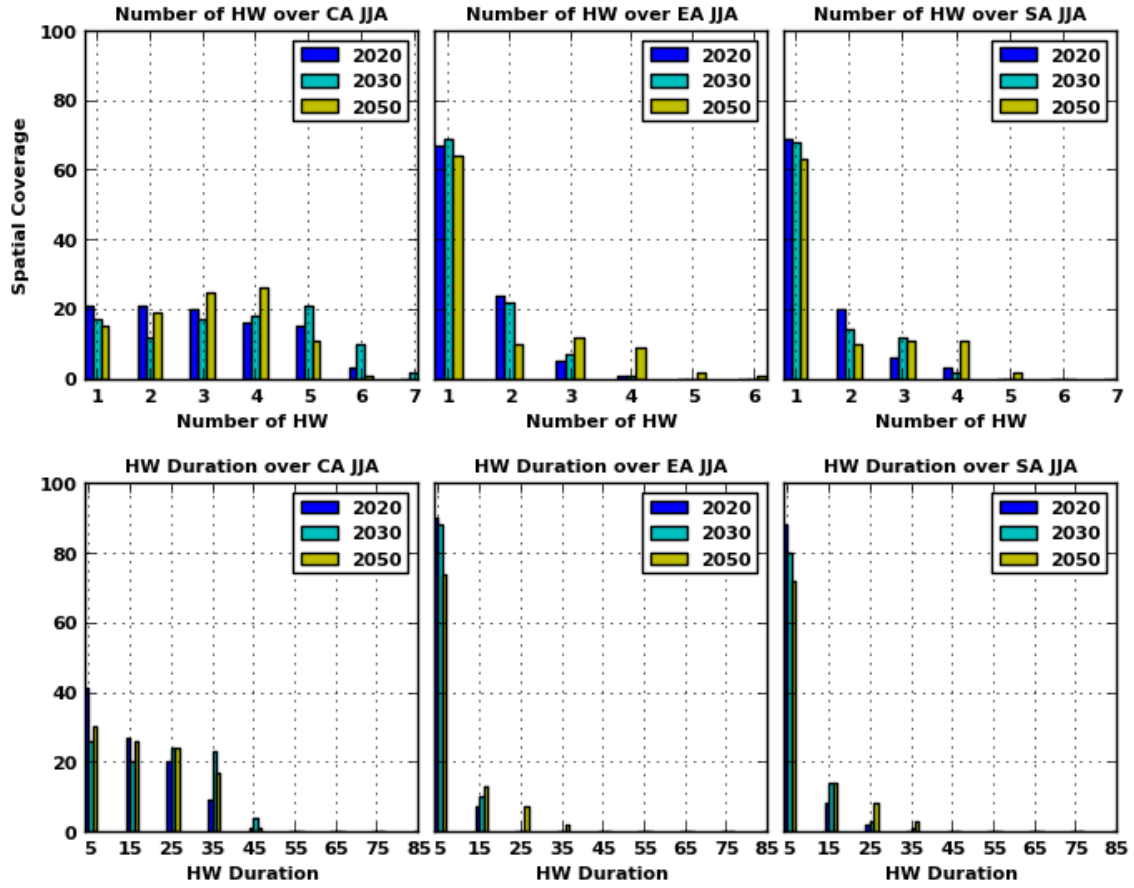
Figure 11. Number of Heat Waves (HW) (top) and duration days (bottom) regarding the Asia regions of CA, EA and SA for 2020 (blue), 2030 (cyan) and 2050 (yellow) during summer months.
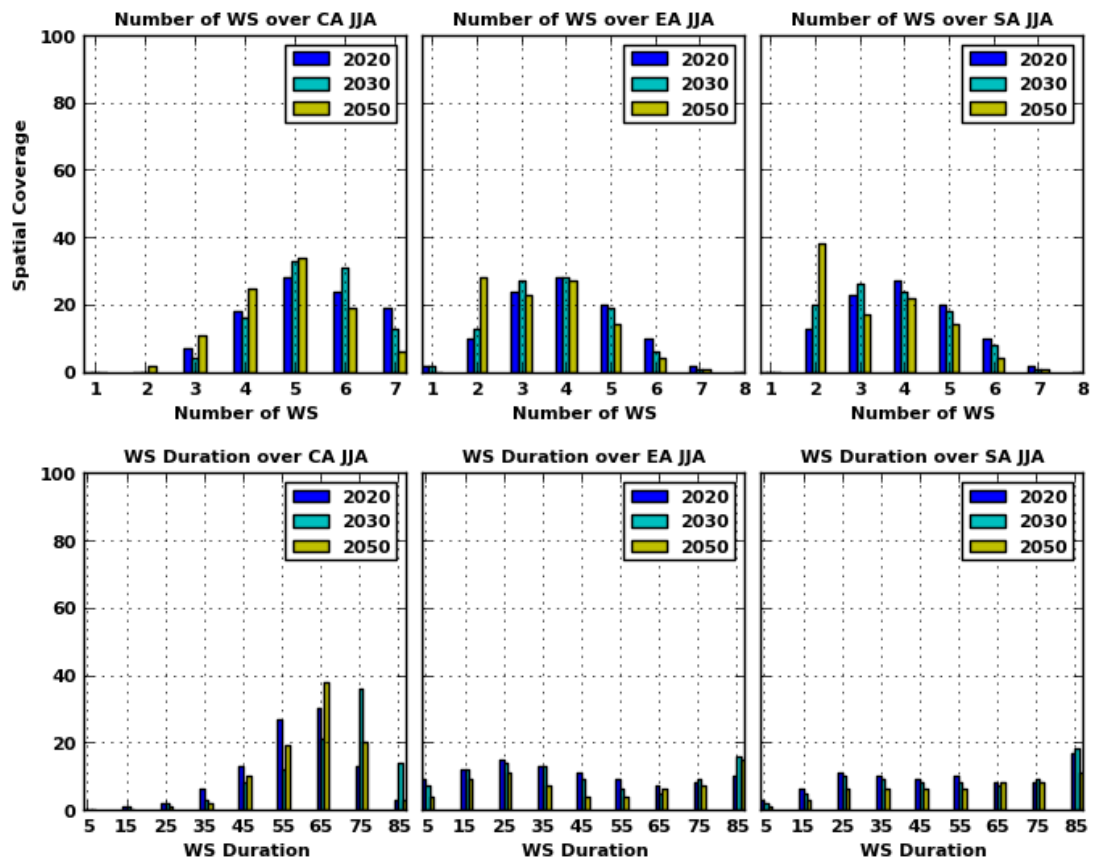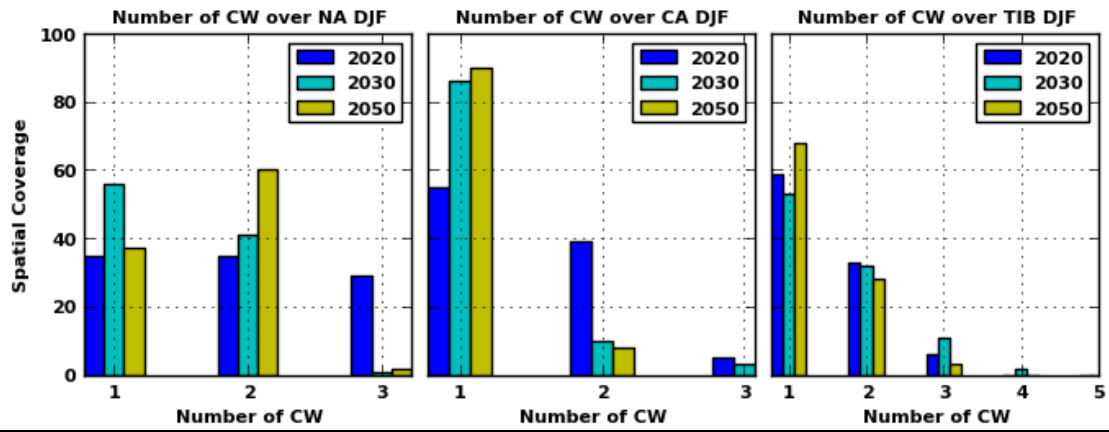
Figure 12. Number of warm spells (top) and duration days (bottom) regarding the Asia regions of CA, EA and SA for 2020 (blue), 2030 (cyan) and 2050 (yellow) during summer months.
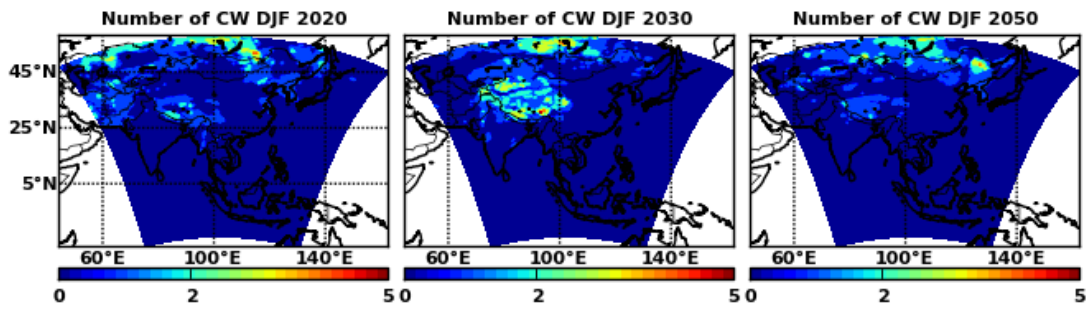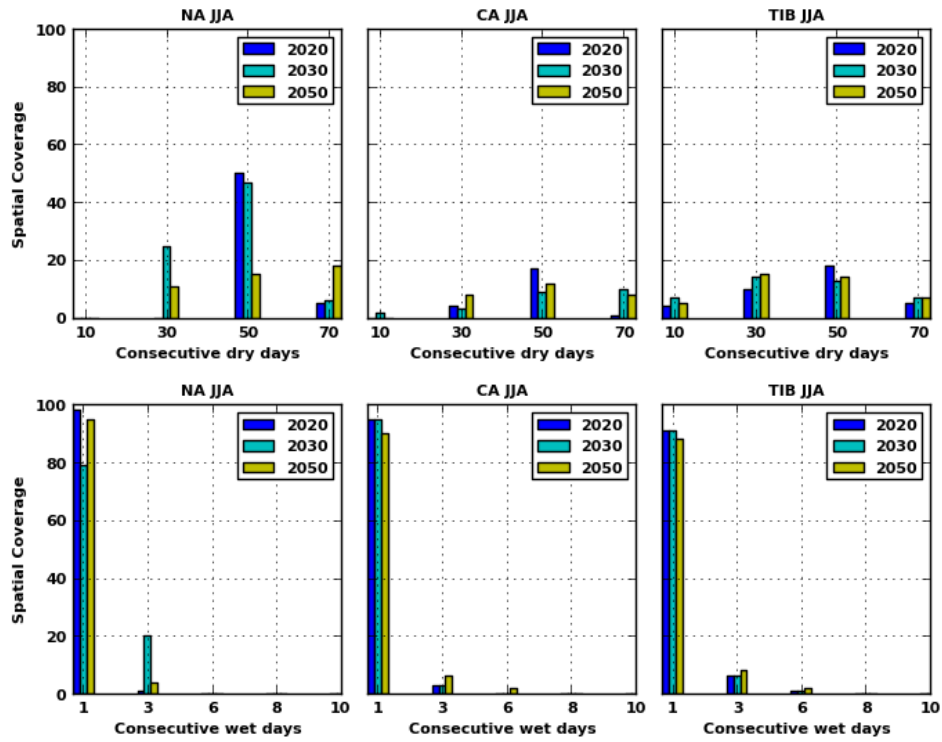
a)

b)

Figure 13. a) Number of Cold Waves (CW) regarding the Asia regions of NA, CA and TIB for 2020 (blue), 2030 (cyan) and 2050 (yellow); and b) duration days for the entire region during winter months.
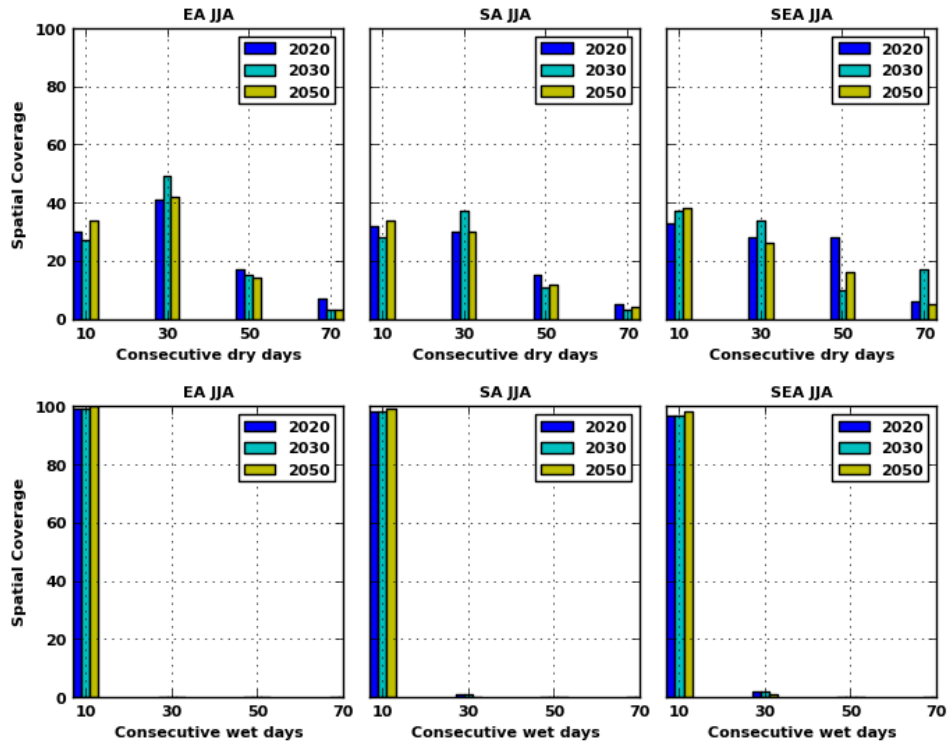
Figure 14. Number of cdd and cwd for the Asia regions of NA, CA, TIB, EA, SA, SEA for 2020 (blue), 2030 (cyan) and 2050 (yellow) during the summer months.

Figure 15. Number strbre for the Asia regions of CA, TIB, EA and SA for 2020 (blue), 2030 (cyan) and 2050 (yellow) during the winter and summer months.

43

Table 1. Configuration of WRF model used in the present study

Dynamics	Non-Hydrostatic
Main Prognostic Variables	u, v, w, t, q and p
Number of grid points	151 x 151 grid points along latitude and longitudinal direction
Horizontal grid distance	54 km
Vertical co-ordinate	Terrain-following hydrostatic-pressure co-ordinate (36 levels)
Cumulus parameterization	Kain–Fritsch mass-flux scheme
Land surface parameterization	NOAH scheme

Cloud microphysics	Thompson scheme
PBL parameterization	YSU scheme
Radiation parameterization	RRTM and Dudhia for long wave and short wave respectively
Horizontal grid distribution	Arakawa C-grid

Table 2. Climate indices used in the present study

Acronym	Definition
cwdi	Cold Wave duration index: Let Tn be the daily series of minimum temperature, TMn be the mean minimum temperatures for the respective season. Cwdi is number of days where, in intervals of at least 6 consecutive days Tn < TMn – 5
cwfi	Cold Spell days: Let TG be the daily series of mean temperature, TG10 be 10th percentile of daily mean temperatures for the respective season. Cwfi is number of days where, in intervals of at least 6 consecutive days TG < TG10
hwdi	Heat Wave duration index: Let Tx be the daily series of maximum temperature, TMx be the mean maximum temperatures for the respective season. Hwdi is

	number of days where, in intervals of at least 6 consecutive days Tx < TMx + 5
hwfi	Warm Spell days index: Let TG be the daily series of mean temperature, TG90 be 90th percentile of daily mean temperatures for the respective season. Hwfi is number of days where, in intervals of at least 6 consecutive days TG > TG90
cdd	Consecutive dry days: Let RR be a time series of daily precipitation amounts, then counted is the largest number of consecutive days where RR is less than 1 mm
cwd	Consecutive wet days: Let RR be a time series of daily precipitation amounts, then counted is the largest number of consecutive days where RR is greater than 1 mm
strwin	Strong wind days: Let VX be a time series of daily maximum horizontal wind speeds, then counted is the number of days where VX > v m/s, where v is an optional value
strbre	Strong Breeze days: Let VX be a time series of daily maximum horizontal wind speeds, then counted is the number of days where VX is greater than or equal to 10.5 m/s
r10	Number of days per year with precipitation above 10 mm: Let RR be a time series of daily precipitation amounts, then counted is the number of days where RR is at least 10 mm

Table 3. Six sub regions used in the study

S.N.	Region Name	lat1 °E	lon1 °N	lat2 °E	lon2 °N
1	North Asia (NA)	50	40	70	80
2	Central Asia (CA)	30	40	50	75
3	Tibetan Plateau (TIB)	30	50	75	100

4	East Asia (EA)	20	100	50	145
5	South Asia (SA)	5	64	50	100
6	South East Asia (SEA)	11	90	20	115

Table 4. Percentage variance for the first 5 EOFs regarding persistent atmospheric anomalies

#EOFs	DJF	MAM	JJA	SON	Annual	#EOFs	DJF	MAM	JJA	SON	Annual
Percentage (%) of variance explained by the first 10 seasonal and annual EOFs regarding Z300hPa						**Percentage (%) of variance explained by the first 10 seasonal and annual EOFs regarding MSLP**					
1	66.2	62.1	40.4	67.2	82.5	1	42.7	38.4	19.6	38.2	59.0
2	9.7	14.7	20.7	13.9	5.9	2	11.8	16.5	15.5	17.9	8.6
3	4.5	5.1	9.6	4.3	2.8	3	7.7	6.2	10.9	7.1	4.7
4	3.8	4.1	5.3	3.6	2.1	4	6.3	5.5	7.3	5.8	3.7
5	3.1	2.6	4.5	2.4	1.4	5	3.7	4.3	5.5	4.7	3.4
Percentage (%) of variance explained by the first 10 seasonal and annual EOFs regarding Tmax						**Percentage (%) of variance explained by the first 10 seasonal and annual EOFs regarding Tmin**					
1	57.4	68.6	29.7	70.3	82.3	1	60.32	63.74	23.39	66.94	80.27
2	6.9	8.4	14.1	8.7	4.5	2	6.36	11.36	12.41	12.05	5.18
3	5.3	2.8	10.2	3.4	2.1	3	4.98	3.50	9.88	2.98	2.79
4	3.4	2.4	6.5	2.7	1.6	4	3.78	1.93	7.01	2.56	1.83
5	2.7	1.7	5.2	1.4	1.3	5	2.76	1.61	5.76	1.58	1.42
Percentage (%) of variance explained by the first 10 seasonal and annual EOFs regarding W10						**Percentage (%) of variance explained by the first 10 seasonal and annual EOFs regarding POV**					
1	13.8	15.8	14.1	15.7	21.7	1	15.4	8.5	8.2	10.7	11.9
2	10.3	8.6	5.9	8.7	6.9	2	5.8	6.9	5.7	6.1	6.2
3	5.9	5.7	5.1	6.3	5.3	3	5.0	4.3	4.5	5.1	4.6
4	4.3	3.6	5.0	3.3	4.6	4	4.4	3.5	3.5	4.1	3.7
5	3.1	3.2	3.5	3.1	2.9	5	3.4	3.0	2.7	3.3	2.7